Articles

Aluminum Phenylphosphonates: A Fertile Family of Compounds

Aurelio Cabeza,[†] Miguel A. G. Aranda,[†] Sebastian Bruque,*[,†] Damodara M. Poojary,[‡,§] Abraham Clearfield,[‡] and Jesus Sanz[||]

Departamento de Química Inorgánica, Universidad de Málaga, 29071 Málaga, Spain, Department of Chemistry, Texas A&M University, College Station, Texas 77843, and Instituto de Ciencia de Materiales, CSIC, Cantoblanco, 28049 Madrid, Spain

Received March 5, 1998

Six aluminum phenylphosphonates have been synthesized depending upon the synthetic conditions: $Al_2(O_3PC_6H_5)_3 \cdot 2H_2O$ (**I**), $Al_2(O_3PC_6H_5)_3$ (**II**), α-$Al(HO_3PC_6H_5)(O_3PC_6H_5) \cdot H_2O$ (**III**), β-$Al(HO_3PC_6H_5)(O_3PC_6H_5) \cdot H_2O$ (**IV**), $Al(HO_3PC_6H_5)_3 \cdot H_2O$ (**V**), and $Al(OH)(O_3PC_6H_5)$ (**VI**). Thermal analysis, X-ray powder thermodiffractometry, IR spectroscopy, and ^{27}Al and ^{31}P MAS NMR data have been obtained to study the structure and thermal stability of these materials. **III** crystallizes in the orthorhombic system, space group *Pbca*, with $a = 9.7952(1)$ Å, $b = 29.3878(4)$ Å, $c = 9.3537(3)$ Å, and $Z = 8$. The structure was solved ab initio, from synchrotron data ($\lambda \approx 0.4$ Å), using direct methods, and refined by Rietveld methods. The final agreement factors were $R_{wP} = 6.73\%$, $R_P = 5.24\%$, and $R_F = 6.8\%$. The compound is layered with the aluminum atoms in an octahedral environment of oxygens and two crystallographically independent phosphonate groups, one being protonated. The powder patterns of **V** and **VI** have been indexed, and the experimental observations are consistent with layered structures. The unit cell of **V** contains one octahedral site for Al and three tetrahedral sites for P. Phosphonate **I** seems to have a three-dimensional tubular structure with aluminum atoms in both octahedral and tetrahedral environments and phosphorus atoms in three different types of sites.

Introduction

The metal phosphonates are a class of inorganic−organic hybrid materials, characterized by the presence of covalent bonds between the inorganic and organic moieties. In this family, the chemistry of metal phosphonates has received increasing attention for the last 15 years. The main research effort in the metal phosphonates field was initially directed toward tetravalent cations. A wide variety of tetravalent metal phosphonates (for instance, Zr, Ti, Sn, and Ce) have been known since the early 1980s.[1] The crystal structure of these materials was assumed to be related to that of α-zirconium phosphate, $Zr(O_3POH)_2 \cdot H_2O$.[2] Later, the structure of zirconium phenylphosphonate, $Zr(O_3PC_6H_5)_2$, was solved from powder diffraction data[3] and the close relationship between the structures became clear. Many other investigations have been reported about the synthesis, crystal structures, and properties of divalent metal phosphonates,[4−8] and more recently about trivalent metal phosphonates.[7b,9,10] The general interest in the chemistry of metal organophosphonates is mainly due to the unusual compositional and structural diversity varying from one-dimensional arrangements to three-dimensional microporous frameworks, passing by the most common layered networks. The importance of such systems in several research areas such as electrochemistry,[11,12] microelectronics,[13] biological membranes,[14,15] photochemical mechanisms[16] and catalysis[17,18] has been widely recognized.

Several studies of trivalent metal phenylphosphonates have been carried out. Two iron(III) derivatives, $FeH(HO_3PC_6H_5)_4$ and $Fe(HO_3PC_6H_5)(O_3PC_6H_5) \cdot H_2O$, were synthesized, and the structure of the first compound was solved from single-crystal data. The main structural features are linear chains with iron

* To whom correspondence should be addressed.
† Universidad de Málaga.
‡ Texas A&M University.
§ Current address: Symyx Technologies, 3100 Central Expressway, Santa Clara, CA 95051.
|| CSIC.

(1) (a) Alberti, G.; Costantino, U.; Allulli, S.; Tomasini, N. *J. Inorg. Nucl. Chem.* **1978**, *40*, 1113. (b) Dines, M. B.; Giacomo, P. D. *Inorg. Chem.* **1981**, *20*, 92−97. (c) Drumel, S.; Penicaud, V.; Deniaud, D.; Bujoli, B. *Trends Inorg. Chem.* **1996**, *4*, 13−25. (d) Clearfield, A. In *Progress in Inorganic Chemistry*; Karlin, K. D.; Ed.; John Wiley: New York, 1998, pp 371−510.
(2) Clearfield, A.; Troup, J. M. *Inorg. Chem.* **1977**, *16*, 3311−3314.
(3) Poojary, D. M.; Hu, H.-L.; Campbell, F. L., III; Clearfield, A. *Acta Crystallogr.* **1993**, *B49*, 996−1001.
(4) Cunningham, D.; Hennelly, P. J.; Deeny, T. *Inorg. Chim. Acta* **1979**, *37*, 95−102.
(5) Cao, G.; Lee, H.; Lynch, V. M.; Mallouk, T. E. *Inorg. Chem.* **1988**, *27*, 2781−2785.
(6) Martin, K. J.; Squattrito, P. J.; Clearfield, A. *Inorg. Chim. Acta* **1988**, *155*, 7−9.
(7) (a) Cao, G.; Lee, H.; Lynch, V. M.; Mallouk, T. E. *Solid State Ionics* **1988**, *26*, 63−69. (b) Cao, G.; Lee, H.; Lynch, V. M.; Swinnea, J. S.; Mallouk, T. E. *Inorg. Chem.* **1990**, *29*, 2112−2117.
(8) (a) Zhang, Y.; Clearfield, A. *Inorg. Chem.* **1992**, *31*, 2821−2826. (b) Bhardwaj, C.; Hu, H.-L.; Clearfield, A. *Inorg. Chem.* **1993**, *32*, 4294−4299.
(9) Bujoli, B.; Palvadeau, P.; Rouxel, J. *Chem. Mater.* **1990**, *2*, 582−589.
(10) Wang, R.; Zhang, Y.; Hu, H.; Frausto, R. R.; Clearfield A. *Chem. Mater.* **1992**, *4*, 864−871.
(11) Murray, R. W. *Acc. Chem. Res.* **1980**, *13*, 135−141.
(12) Facci, J. S. *Langmuir* **1987**, *3*, 525−530.

S0020-1669(98)00235-3 CCC: $15.00
Published on Web 08/06/1998

atoms in an octahedral coordination of oxygens.[9] The structure of the second compound could not be determined although it seems to be related to that of α-ZrP. A series of phenyl- and benzylphosphonates of the lanthanide elements were reported, and the structures of $La(HO_3PC_6H_5)(O_3PC_6H_5)$ and $La(HO_3PCH_2C_6H_5)(O_3PCH_2C_6H_5)\cdot 2H_2O$ were solved from single-crystal data.[10] The synthesis of a second type of rare-earth phenylphosphonates of general composition $Ln_2(O_3PC_6H_5)_3$ was also reported.[10] Other reports describing trivalent metal phosphonates are those of V organodiphosphonates,[19] the series of compounds with general formula $LnH(O_3PR)_2$ (R = alkyl, phenyl; Ln = La, Sm, Ce),[8] and bismuth (carboxyethyl)-phosphonate.[20]

There are several reports dealing with aluminum phosphonates. The research effort has been focused on phenyl- and methylphosphonates. $Al_2(O_3PCH_3)_3$[21] has at least two polymorphic forms. The phases show a tridimensional structure with unidimensional channels, in which the methyl groups are situated toward the interior of the pores, resulting in hydrophobic microtubes.[22,23] A layered aluminum methylphosphonate, $AlOH(O_3PCH_3)\cdot H_2O$, has also been reported,[24] and two aluminum phenylphosphonates were very recently reported, $Al(HO_3PC_6H_5)(O_3PC_6H_5)_2\cdot H_2O$[25] and $Al_2(O_3PC_6H_5)_3\cdot 4H_2O$,[26] although their crystal structures were not determined.

In this paper, we report on a study of the Al(III) phenylphosphonate system. Six phosphonates have been isolated, depending upon the synthetic conditions. One structure has been solved ab initio from powder diffraction data, and ^{27}Al and ^{31}P MAS NMR and powder X-ray thermodiffractometry have been used to gain some insights into the structures of these materials.

Experimental Section

Chemicals of reagent quality were obtained from commercial sources and were used without further purification. The synthesized phosphonate samples were dissolved in HNO_3 (1/1), and the aluminum content was determined by atomic absorption spectrometry. Carbon and hydrogen contents were determined by elemental chemical analysis in a Perkin-Elmer 240 analyzer. The phosphorus content was deduced from the carbon percentage found, assuming a C/P molar ratio of 6/1. The water content was determined from the weight loss in the heating process.

Thermal analysis (TGA and DTA) was carried out in air on a Rigaku Thermoflex apparatus at a heating rate of 10 K min^{-1} with calcined Al_2O_3 as reference. IR spectra were recorded on a Perkin-Elmer 883 spectrometer in the spectral range 4000−400 cm^{-1}, by using KBr pellets.

Room-temperature powder diffraction patterns were collected with a Siemens D-5000 automated diffractometer using graphite-monochromated Cu Kα radiation. The powder thermodiffractometric studies were carried out with the same diffractometer but in a second goniometer permanently equipped with an HTK10 heating chamber. The samples were mounted directly on Pt foil, which is both the heating system and the holder. The thermodiffractometric patterns were scanned over the angular range 3−38° (2θ), with a step size of 0.05° and counting 1 s per step. The appropriate heating and cooling temperatures were selected by using the Diffract AT software. Samples were held at temperature 10 min, before recording any pattern, to ensure that any transformations that may take place were allowed time to complete.

For $Al(HO_3PC_6H_5)(O_3PC_6H_5)\cdot H_2O$, high-resolution synchrotron powder data were collected on the diffractometer of the BM16 line of ESRF. The sample was loaded into a borosilicate glass capillary ($\phi = 0.5$ mm) and rotated during data collection. The pattern was collected with $\lambda = 0.39989(2)$ Å, in the angular range 1−30° in 2θ, for an overall counting time of 10 h. Further experimental details regarding data collection have already been reported.[27]

^{27}Al and ^{31}P MAS NMR spectra were recorded at 104.26 and 161.98 MHz, respectively, with a Bruker MSL-400 spectrometer. The external magnetic field was 9.4 T. All measurements were carried out at 295 K, and the samples were spun around the magic angle (54°44′ with respect to the magnetic field) at a spinning rate of 12 kHz. The NMR spectra were obtained after $\pi/8$ (Al signal) and $\pi/2$ (P signal) excitations (2 and 4 μs, respectively) and intervals between successive accumulations of 5 and 30 s in both signals. The ^{27}Al and ^{31}P chemical shift values are given relative to 1 M $AlCl_3$ and 85% H_3PO_4 aqueous solutions, respectively. In all cases, the mean error on chemical shift values of components was lower than 0.3 ppm. The deconvolution of the MAS NMR spectra was carried out by using the WINFIT program (from Bruker) in order to determine the shape and intensities of the components.

Synthesis of $Al_2(O_3PC_6H_5)_3\cdot 2H_2O$ (I). Two solutions which contained respectively 7.43 mmol of $H_2O_3PC_6H_5$ in absolute ethanol and 1.48 mmol of anhydrous $AlCl_3$ in absolute ethanol were mixed (P/Al molar ratio: 5/1). The mixture had a pH of <3 to avoid the hydrolysis of aluminum, and it was refluxed for a week (final volume 40 mL). The resulting white suspension was centrifuged, washed with ethanol several times, dried in air, and stored at 58% relative humidity (atmosphere from 40% w/w aqueous H_2SO_4). Anal. Found: Al, 9.43; P, 16.66; C, 38.76; H, 3.49. Calcd for **I**: Al, 9.67; P, 16.65; C, 38.72; H, 3.41. When **I** is heated above 80 °C, it is dehydrated to give $Al_2(O_3PC_6H_5)_3$ **(II)**.

Synthesis of (a) α-$Al(HO_3PC_6H_5)(O_3PC_6H_5)\cdot H_2O$ (III). A 1.27 mmol sample of $AlCl_3\cdot 6H_2O$ and 12.66 mmol of $H_2O_3PC_6H_5$ (P/Al molar ratio: 10/1) were dissolved in 30 mL of water, and then 2 mL of 30% NaOH was added. The mixture was introduced into a 50 mL Teflon-lined autoclave, which was sealed and placed in an oven at 200 °C for 9 days. A single-phase sample was isolated by filtration, washed with water and acetone, and finally dried under vacuum. Anal. Found: C, 40.35; P, 17.37; H, 3.65. Calcd for **III**: C, 40.22; P, 17.31; H, 3.63.

(b) β-$Al(HO_3PC_6H_5)(O_3PC_6H_5)\cdot H_2O$ (IV). To 25 mL of a 0.1 M solution of $Al_2(SO_4)_3\cdot 18H_2O$ was added 3.9525 g of $H_2O_3PC_6H_5$ dissolved in 25 mL of water (P/Al molar ratio: 10/1). The pH was increased from 1 to 1.5 through addition of 30% aqueous NaOH, resulting in the precipitation of a white solid. The total mixture was heated in a Teflon-lined autoclave at 200 °C for 3 days. A single powdered phase was isolated by filtration. The powder diffraction pattern of **IV** was different from that shown by **III**. Anal. Found: C, 41.28; P, 17.85; H, 3.44. Calcd for **IV**: C, 40.22; P, 17.31; H, 3.63.

(13) Roberts, G. G. *Adv. Phys.* **1985**, *34*, 475−512.
(14) Ringsdorf, G.; Schmidt, X.; Schneider, J. *Thin Solid Films* **1987**, *152*, 207−222.
(15) Fendler, J. H. *Membrane Mimetic Chemistry*; Wiley: New York, 1982.
(16) (a) Gratzel, M. *Pure Appl. Chem.* **1982**, *54*, 2369. (b) Thomas, J. K. *Acc. Chem. Res.* **1988**, *21*, 275−280. (c) Colon, J. L.; Yang, C.-Y.; Clearfield, A.; Martin, C. R. *J. Phys. Chem.* **1988**, *92*, 5777; **1990**, *94*, 874. (d) Vermeulen, L. A.; Thompson, M. E. *Nature* **1992**, *358*, 656. (e) Vermeulen, L. A.; Snover, J. L.; Sapochak, L. S.; Thompson, M. E. *J. Am. Chem. Soc.* **1993**, *115*, 11767−11774. (f) Poojary D. M.; Vermeulen, L. A.; Vicenzi, E.; Clearfield, A.; Thompson, M. E. *Chem. Mater.* **1994**, *6*, 1848.
(17) Soghomonian, V.; Haushalter C.; Zubieta, J. *Chem. Mater.* **1995**, *7*, 1648−1654.
(18) Janvier P.; Drumel, S.; Piffard, Y.; Bujoli, B. *C. R. Acad. Sci. Ser. II* **1995**, *320*, 29−35.
(19) (a) Maeda, K.; Kiyozumi, Y.; Mizukami, F. *Angew. Chem., Int. Ed. Engl.* **1994**, *33*, 2335−2337. (b) Maeda, K.; Kiyozumi, Y.; Mizukami, F. *J. Phys. Chem. B* **1997**, *101*, 4402−4412. (c) Carter, V. J.; Wright, P. A.; Gale, J. D.; Morris, R. E.; Sastre, E.; Perez-Pariente, J. *J. Mater. Chem.* **1997**, *7*, 2287−2292.
(20) Maeda, K.; Akimoto, J.; Kiyozumi, Y.; Mizukami, F. *Angew. Chem., Int. Ed. Engl.* **1995**, *34*, 1199−2001.
(21) Maeda, K.; Akimoto, J.; Kiyozumi, Y.; Mizukami, F. *J. Chem. Soc., Chem. Commun.* **1995**, 1033−1034.
(22) Sawers L. J.; Carter, J. V.; Armstrong, A. R.; Bruce, P. G.; Wright, P. A.; Gore, B. E. *J. Chem. Soc., Dalton Trans.* **1996**, 3159−3161.
(23) Haky, J. E.; Brady, J. B.; Dando N.; Weaver, D. *Mater. Res. Bull.* **1997**, *32*, 297−303.
(24) Raki, L.; Detellier, C.; *Chem. Commun.* **1996**, *21*, 2475−2476.
(25) Aranda, M. A. G.; Losilla, E. R.; Cabeza, A.; Bruque, S. *J. Appl. Crystallogr.* **1998**, *31*, 16−21.

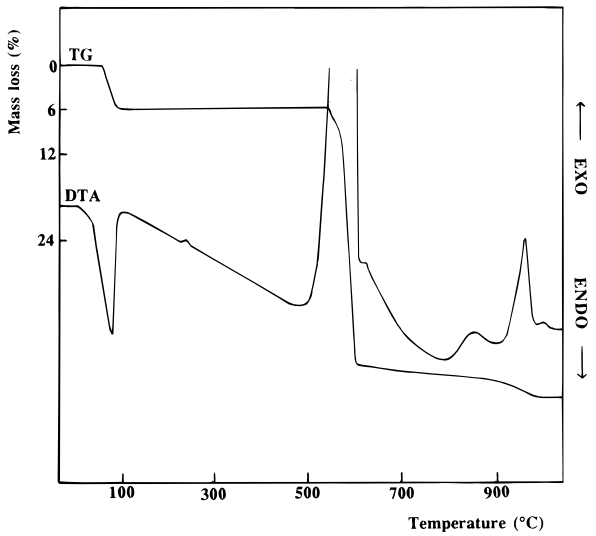

Figure 1. TGA−DTA curves for $Al_2(O_3PC_6H_5)_3 \cdot 2H_2O$.

Synthesis of $Al(HO_3PC_6H_5)_3 \cdot H_2O$ (V). A mixture of 3.79 mmol of anhydrous $AlCl_3$ and 18.97 mmol of $H_2O_3PC_6H_5$ (P/Al molar ratio: 5/1) in 50 mL of toluene was refluxed in a round-bottom flask for 2 weeks. The product was isolated by filtration as a white powder. It was washed with ethanol and acetone several times and dried in air. Anal. Found: Al, 4.5; C, 43.37; P, 18.67; H, 3.87. Calcd for **V**: Al, 5.3; C, 41.86; P, 18.02; H, 3.64.

Synthesis of $Al(OH)(O_3PC_6H_5)$ (VI). To 25 mL of an aqueous solution containing 18.96 mmol of $AlCl_3 \cdot 6H_2O$ was added 25 mL of a 0.25 M solution of $H_2O_3PC_6H_5$ (P/Al molar ratio: 1/3). Initially no precipitate was formed. The resulting solution was introduced into a Teflon-lined autoclave, with stirring, and heated at 200 °C for 5 days. A white powder was isolated by filtration. It was washed with water and acetone several times and dried in air. This compound can also be obtained from $Al_2(O_3PC_6H_5)_3 \cdot 2H_2O$ **(I)** by heating 170 mg with 30 mL of water in an autoclave at 200 °C for 10 days. Anal. Found: C, 35.29; P, 15.19; H, 2.40. Calcd for **VI**: C, 35.98; P, 15.49; H, 2.99.

Results

Thermal Study. (a) $Al_2(O_3PC_6H_5)_3 \cdot 2H_2O$. TGA−DTA curves for **I** are shown in Figure 1. One endothermic event centered at 80 °C and three exotherms centered at 600, 840, and 950 °C are observed. The endothermic effect has an associated weight loss of 6.4%, which corresponds to the release of the two water molecules (calculated mass loss 6.45%). The first strong exotherm is due to the combustion of the organic groups. The other two exothermic effects correspond to crystallizations and decompositions. The total mass loss at 1050 °C, 46.2%, is slightly larger than the theoretical value, 43.6%, deduced from the overall thermal decomposition reaction (1).

$$2Al_2(O_3PC_6H_5)_3 \cdot 2H_2O + 45O_2 \rightarrow Al(PO_3)_3 + 3AlPO_4 + 36CO_2 + 19H_2O \quad (1)$$

The X-ray powder diffraction pattern of the sample heated at 750 °C is amorphous with some low-intensity peaks. However, the pattern of the sample heated at 1050 °C is crystalline and shows diffraction peaks which correspond to $Al(PO_3)_3$ and $AlPO_4$ (PDF database nos. 13-0430 and 11-0500, respectively). There are also some very small peaks which belong to a third unidentified phase, which may be responsible for the difference between the observed and calculated overall mass losses.

A thermodiffractometric study (Figure 2) was undertaken to characterize the water loss of compound **I**. Compound **I** is only stable up to 40 °C, above which it begins to lose water. Between 45 and 55 °C, **I** and **II** coexist, and at 60 °C a single phase of **II** is observed. Although **II** is present at room temperature on cooling, we have observed by X-ray powder diffraction, that the rehydration process does take place partially over several days, by absorbing water from the atmosphere. It is important to point out that the most intense peak for I, at 13.2 Å, is displaced to 11.7 Å after the weight loss. Simultaneously, the highest *d*-spacing peak moves from 26.1 to 23.2 Å and its relative intensity increases notably.

(b) α-$Al(HO_3PC_6H_5)(O_3PC_6H_5) \cdot H_2O$. The DTA-TGA curves for **III** are shown in Figure 3. The first endotherm centered at 183 °C is due to the loss of hydration water (the observed and calculated weight losses are 6.0 and 5.0%, respectively). There are three small endotherms at 235, 275, and 310 °C, without mass losses, which must be due to subtle phase transitions. The second mass loss is due to the pyrolysis of the phenyl groups, and it can be seen as a main endotherm at 537 °C with two small associated endotherms at 400 and 460 °C. The overall observed mass loss, 45.5%, agrees well with the theoretical loss of 46.1% deduced from the overall thermal decomposition reaction (2). There is no evidence of combustion of the organic radicals in air as no exothermal effect is observed in the DTA curve.[9,38]

$$2\alpha\text{-}Al(HO_3PC_6H_5)(O_3PC_6H_5) \cdot H_2O + O_2 \rightarrow Al_2O_3 \cdot 2P_2O_5 + 3H_2O + [4C_6H_5] \quad (2)$$

The X-ray powder diffraction pattern of the sample heated at 800 °C showed no peaks, indicating that the thermal decomposition of **III** leads to a glassy solid. The loss of the hydration water was studied by powder thermodiffractometry (Figure 4). Above 160 °C, the water is lost, and the resulting powder patterns have much broader peaks and much lower intensities. It is important to underline that the *d*-spacing value for the first reflection (020), 14.6 Å, does not change during this process. On heating, there are no further changes in the powder pattern although several endotherms are evident in the DTA curve of this material.

(c) $Al(HO_3PC_6H_5)_3 \cdot H_2O$. The DTA−TGA curves for **V** are given in Figure 5. The first endotherm centered at 240 °C, with an associated mass loss of 4.0%, corresponds to the release of the water molecule (calculated value 3.5%). There are two endotherms at 470 and 512 °C, which are due to the pyrolysis of the phenyl organic groups. As observed for α-$Al(HO_3$-

(26) Garvey, R. LATTPARM autoindexing program. Department of Chemistry, North Dakota State University, Fargo, ND 58105-5516. Based on the Visser algorithm: Visser, L. W. *J. Appl. Crystallogr.* **1969**, *2*, 89.
(27) Werner, P. E.; Eriksson, L.; Westdahl, M. *J. Appl. Crystallogr.* **1985**, *18*, 367−370.
(28) Le Bail, A.; Duroy, H.; Fourquet, J. L. *Mater. Res. Bull.* **1988**, *23*, 447−452.
(29) Larson, A. C.; von Dreele, R. B. *(Program version: PC, summer 96). Los Alamos Natl. Lab. [Rep.] LA (U.S.)* **1994**, *LA-UR-86-748*.
(30) Thompson, P.; Cox, D. E.; Hasting, J. B. *J. Appl. Crystallogr.* **1987**, *20*, 79−83.
(31) Finger, L. W.; Cox, D. E.; Jephcoat, A. P. *J. Appl. Crystallogr.* **1994**, *27*, 892−900.
(32) Altomare, A.; Cascarano, G.; Giacovazzo, C.; Guagliardi, A.; Burla, M.; Polidori, G.; Camalli, M. SIRPOW.92. *J. Appl. Crystallogr.* **1994**, *27*, 435−436.
(33) Dollase, W. A. *J. Appl. Crystallogr.* **1986**, *19*, 267.
(34) Rietveld, H. M. *J. Appl. Crystallogr.* **1969**, *2*, 65−71.
(35) Morris, M. C.; McMurdie, H. F.; Evans, E. H.; Paretzkin, B.; deGroot, J. H.; Newberry, R.; Pyrros, N. P.; Hubbard, C. R.; Carmel, S. *NBS Monogr. (U.S.)* **1977**, No. *25*, 1−5.
(36) Poojary, D. M.; Baolong, Z.; Cabeza, A.; Aranda, M. A. G.; Bruque, S.; Clearfield, A. *J. Mater. Chem.* **1996**, *6*, 639−644.

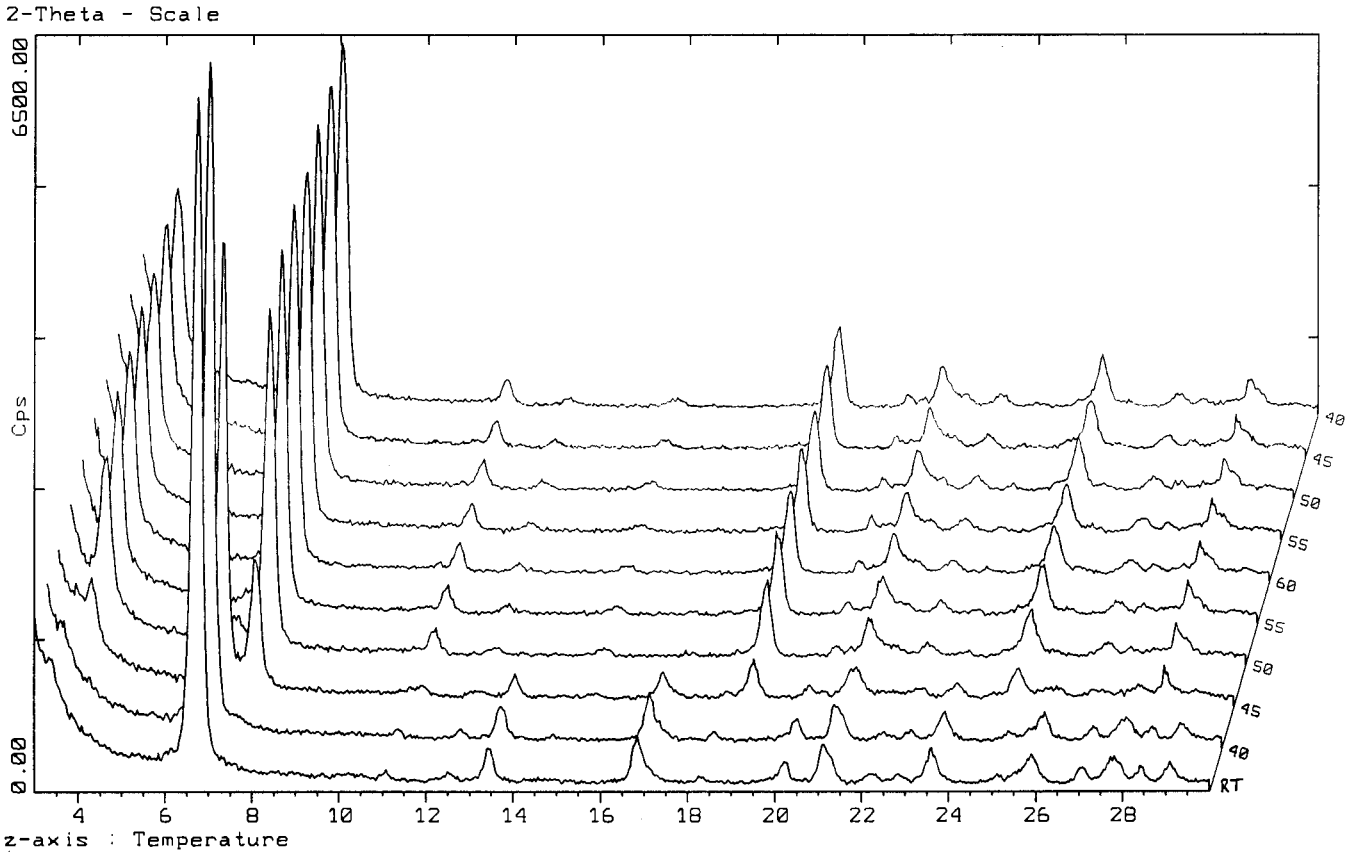

Figure 2. X-ray thermodiffractometric powder patterns for $Al_2(O_3PC_6H_5)_3 \cdot 2H_2O$.

$PC_6H_5)(O_3PC_6H_5) \cdot H_2O$, there is no evidence of combustion of the organic radicals in air in the DTA curve. The overall observed mass loss, 50.0%, is in good agreement with the theoretical value, 48.8%, deduced from the overall thermal decomposition reaction (3).

$$2Al(HO_3PC_6H_5)_3 \cdot H_2O + {}^3/_2O_2 \rightarrow Al_2O_3 \cdot 3P_2O_5 + 5H_2O + [6C_6H_5] \quad (3)$$

The powder pattern of the sample heated at 800 °C also showed no peaks, indicating that the thermal decomposition of **V** results in an amorphous solid. The loss of the hydration water was also studied by powder thermodiffractometry (Figure 6). Above 210 °C, the water is lost; the resulting powder patterns have fewer peaks, and they are broader. The *d*-spacing value for the first reflection (020), 14.5 Å, does not change during the dehydration process (as for **III**), but a large new reflection is present at $2\theta \approx 7°$.

For both α-$Al(HO_3PC_6H_5)(O_3PC_6H_5) \cdot H_2O$ and $Al(HO_3PC_6H_5)_3 \cdot H_2O$ samples, the thermal decomposition reactions including oxygen and organic radicals are possible processes compatible with the observed mass losses. However, further studies are needed to confirm this suggested mechanism and to rule out other decomposition reactions. For example, with the experimental data it is not possible to discard a decompositional reaction without oxygen participation. However, in this case, the vitreous phosphates should contain phosphorus in V and III oxidation states with overall stoichiometries $Al_2O_3 \cdot P_4O_8$ and $Al_2O_3 \cdot P_6O_{12}$, respectively.

(d) $Al(OH)(O_3PC_6H_5)$ (VI). The DTA−TGA curves for **VI** are given in Figure 7. Two endothermic events, centered at 280 and 400 °C, and two exothermic events, at 660 and 730 °C, are observed. The first endotherm has an associated mass loss of 4.4%. This value is very closed to that calculated for the condensation of two hydroxide groups, 4.5%, of $Al(OH)(O_3PC_6H_5)$ to release a water molecule. This transformation causes an increment in the *d* spacing of the first diffraction peak from 16.45 to 17.36 Å. The second endotherm, without mass loss, must be due to subtle phase transitions. The exothermic effects correspond to the combustion of the phenyl groups.

The powder pattern of a sample obtained by heating **VI** at 1000 °C is amorphous, with some low-intensity peaks. However, when the sample is heated to 1100 °C for 2 h, the resulting compound is crystalline and it shows diffraction peaks which mainly correspond to $AlPO_4$ (PDF no. 20-0045). The overall experimental weight loss is 40.8%, in good agreement with the theoretical weight loss of 39.02% for the decomposition reaction (4).

$$Al(OH)(O_3PC_6H_5) + {}^{15}/_2\,O_2 \rightarrow AlPO_4 + 3H_2O + 6CO_2 \quad (4)$$

IR Spectroscopic Study. The IR spectra were recorded between 4000 and 400 cm^{-1} and are shown in Figure 8 between 4000 and 1400 cm^{-1}. This region was selected to study in detail the hydration water and the H−O−P groups. In Figure 8a−d are shown the spectra for **I**, **III**, **V**, and **VI**, respectively. One important feature in the IR spectra is the band observed at 2340 cm^{-1} for **V** (curve c) that appears as a shoulder near 2400 cm^{-1} for **III** (curve b) and is absent for **I** and **VI** (curves, a and d, respectively). This band is characteristic of the hydrogen phenylphosphonate groups and it is more intense for compound **V**, which has three such groups per formula. The bending H−O−H vibration of the hydration water located at ∼1620 cm^{-1} is always partially overlapped with the sharp band due to the phenyl group stretchings (ν_{C-C}) at 1595 cm^{-1}. The bands

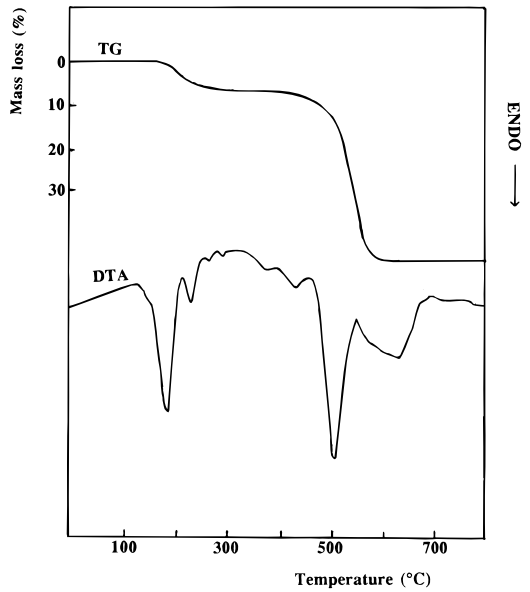

Figure 3. TGA−DTA curves for α-Al($HO_3PC_6H_5$)($O_3PC_6H_5$)·H_2O.

at 1490 and 1440 cm^{-1} are due to the skeletal vibrations of the rings, and the bands at 3000 cm^{-1} are due to the C−H stretching vibrations.

All spectra, except that of **VI**, show an intense and broad band in the O−H stretching vibration region between 3600 and 3200 cm^{-1}, which it is consistent with the presence of hydration water. The IR spectrum for **I** has two bands in this region, one very sharp located at 3640 cm^{-1} and another broader near 3510 cm^{-1}. The sharp band is probably due to a zeolitic water that does not interact by H-bonding, and the position of the second broader band clearly indicates that this water molecule interacts weakly through H-bonds. When **I** is heated above 100 °C to give **II**, these bands and that due to the H−O−H bending vibration disappear. The IR spectrum for **III** presents one band at 3415 cm^{-1}, showing that the water interacts notably by H-bonding, and another at 3070 cm^{-1}, due to the OH group. The IR spectrum for **V** has a main band at 3250 cm^{-1} with a shoulder at 3500 cm^{-1}, showing that this water interacts quite strongly by H-bonding. Compound **VI** shows a strong sharp band at 3660 cm^{-1}, characteristic of the stretching vibration of the hydroxide groups (ν_{O-H}), and no band is observed in the H−O−H bending region, close to 1640 cm^{-1}.

Crystal Structure Study. (a) $Al_2(O_3PC_6H_5)_3 \cdot 2H_2O$. This phosphonate shows a high *d*-spacing value for the first reflection, 26.3 Å. This peak is very sensitive to the humidity, and its *d* spacing decreases quickly to give **II** when it is placed in a dry atmosphere or is heated above 50 °C. The compound has to be stored in a controlled humidity environment (i.e. H_2SO_4, 40%) to avoid the loss of water.

The X-ray powder patterns for both phases (Figure 2) do not show sharp diffraction peaks mainly due to the small size of the crystallites. This problem and the complexity of the structure (with a very large unit cell) have made it difficult to index the patterns. LATTPARM[28] and TREOR90[29] autoindexing programs suggested several possible solutions. We have selected those shown below because they result in good values of volume per atom (V_{at}) and they show a clear relation between the hydrated and anhydrous phases. However, higher crystalline samples or single-crystal data are necessary to verify these initial indexings. The powder pattern of **I** was indexed in a hexagonal unit cell, with parameters $a = 29.17(1)$ Å, $c = 26.38(1)$ Å, and $V = 19440$ $Å^3$. The powder pattern of **II** was indexed in a hexagonal unit cell, with parameters $a = 29.94(1)$ Å, $c = 23.44(1)$ Å, and $V = 18195$ $Å^3$. The observed decrease in the unit

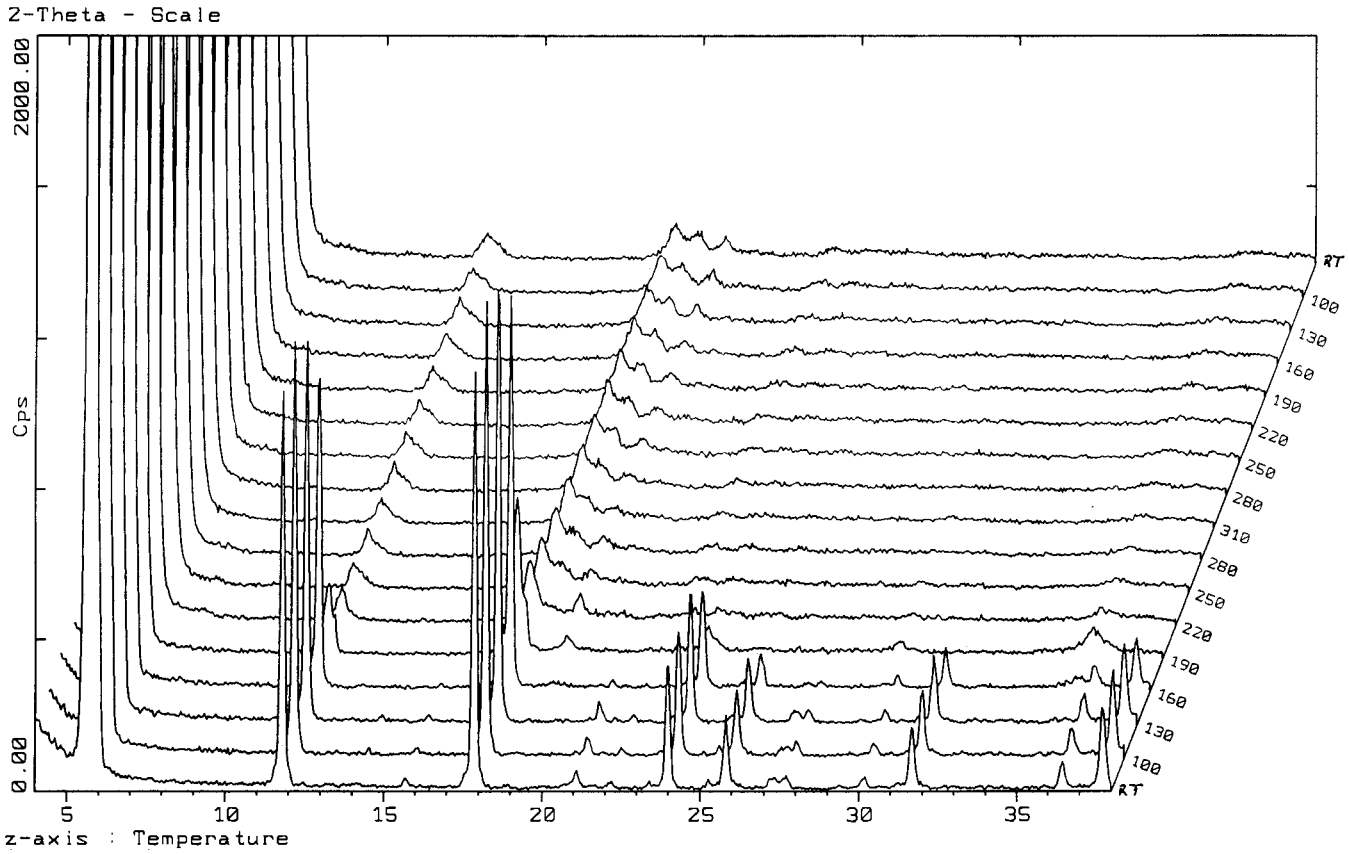

Figure 4. X-ray thermodiffractometric powder patterns for α-Al($HO_3PC_6H_5$)($O_3PC_6H_5$)·H_2O.

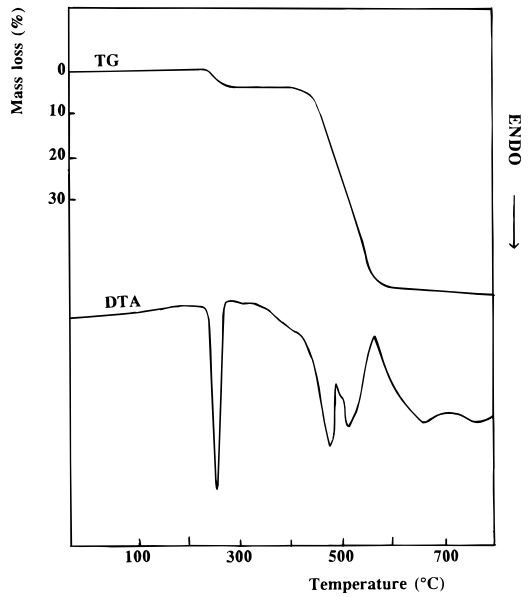

Figure 5. TGA−DTA curves for $Al(HO_3PC_6H_5)_3 \cdot H_2O$.

cell volume after the dehydration process (17.4 Å^3 per H_2O molecule) is consistent with the water loss.

(b) α-$Al(HO_3PC_6H_5)(O_3PC_6H_5) \cdot H_2O$. The X-ray laboratory powder pattern of **III** was autoindexed using the LATTPARM autoindexing program, giving an orthorhombic unit cell with $a = 9.798$ Å, $b = 29.387$ Å, $c = 9.372$ Å, $V = 2698$ Å^3, $Z = 8$, $V_{at} = 15.3$ Å^3/atom, and $M_{20} = 14$. The X-ray powder diffraction data exhibit strong preferred orientation. Hence, intensities are not reliable and it is better to calculate the powder diffraction intensities from the structural model given below. Systematic absences indicated the space group *Pbca* (No. 61). The powder pattern of β-$Al(HO_3PC_6H_5)(O_3PC_6H_5) \cdot H_2O$ **(IV)** is similar to that already published,[25] and therefore, it is not reported here. The powder patterns of these two phases are clearly different, indicating two distinct crystal structures. Although the basal spacings are quite similar for both polymorphs, the (*hkl*) reflections are different, indicating different intralayer atomic arrangements. It is worthwhile to point out that diffraction peaks are sharper in the α polymorph than in the β-phase which reflects a better crystallized α sample.

The crystal structure of compound **III** was solved from high-resolution powder synchrotron diffraction data. The structure factor amplitudes were extracted from a limited region of the diffractogram ($2 < 2\theta < 21.2°$) using the Le Bail method[30] with the pattern decomposition option of the GSAS package.[31] The pattern was fitted without any structural model by refining the following parameters: zero-point error, unit cell, and peak shape. In this case, the pseudo-voight peak shape function[32] was used together with the asymmetry correction of Finger, Cox, and Jephcoat.[33] The background was fitted manually because of the presence of a small amount of amorphous matter. A total of 1140 reflections were used as input to the direct methods of the SIRPOW.92 program.[34] An *E* map calculated for a set with the best figure of merit (CFOM = 0.78) yielded the position of the two phosphorus atoms and the aluminum atom. The positions of these atoms were used as a starting model in the Rietveld refinement using the overall parameters obtained in the last cycle of the Le Bail extraction. We then came back to the Rietveld method. With the inclusion of these three atoms and refining only the scale factor, R_{wP} dropped to 33%. At this stage, a difference Fourier map revealed all the oxygen atoms as well as the two carbon atoms bonded to the two crystallographically independent phosphorus atoms. No other atoms were found from a difference Fourier map. So, the rest

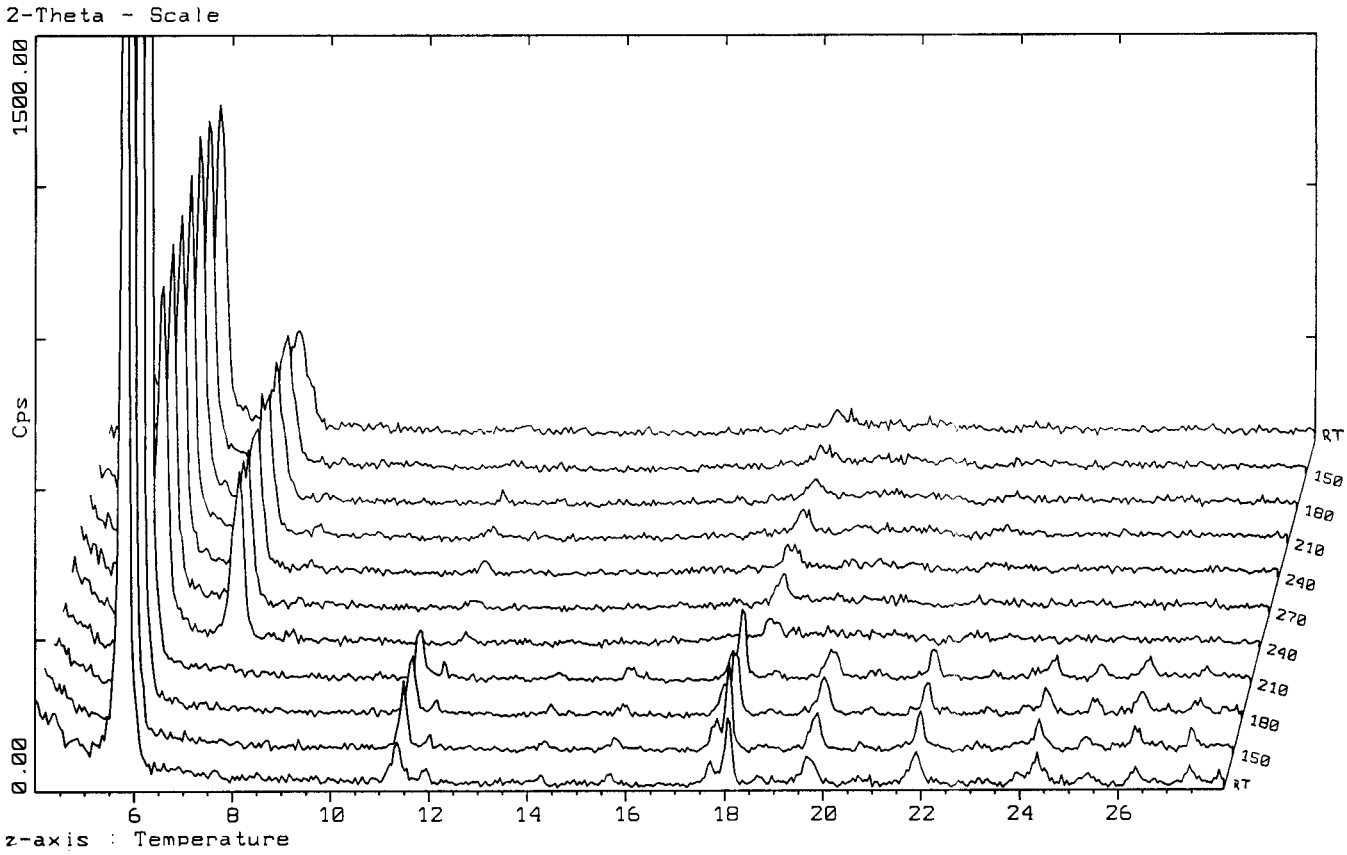

Figure 6. X-ray thermodiffractometric powder patterns for $Al(HO_3PC_6H_5)_3 \cdot H_2O$.

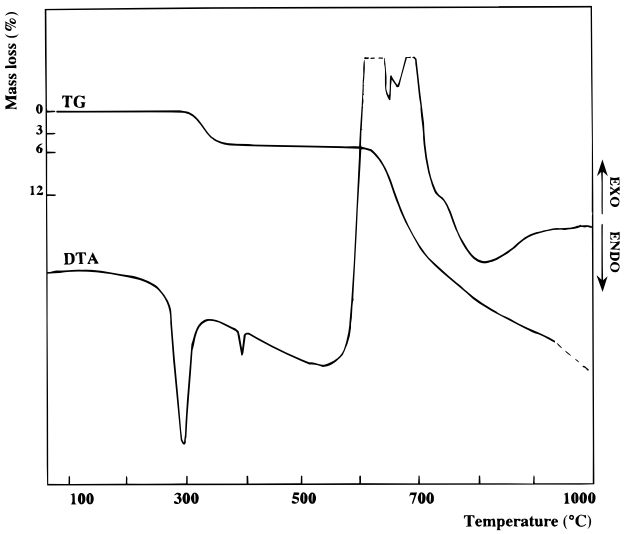

Figure 7. TGA−DTA curves for $Al(OH)(O_3PC_6H_5)$.

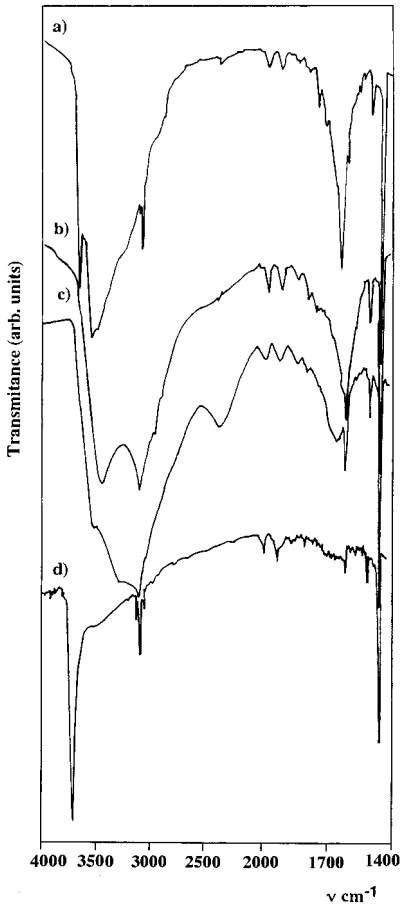

Figure 8. IR spectra for (a) $Al_2(O_3PC_6H_5)_3{\cdot}2H_2O$, (b) α-$Al(HO_3PC_6H_5)(O_3PC_6H_5){\cdot}H_2O$, (c) $Al(HO_3PC_6H_5)_3{\cdot}H_2O$, and (d) $Al(OH)(O_3PC_6H_5)$.

of the carbon atoms were modeled, as they belong to two phenyl groups, and they were included in their calculated positions. At this stage, the refinement of this model was carried out using soft constraints to keep a reasonable geometry for the CPO_3 tetrahedron and the phenyl rings. The following soft constraints were used. Bonding distances: P−O, 1.53(1) Å; P−C, 1.80(1) Å; C−C, 1.40(1) Å. Nonbonding distances: C···C, 2.40(1) Å; C···C, 2.78(1) Å. Initially, the weight for the soft constraints was high, −1500, but it was reduced as the refinement progressed. Under these conditions, the refinement converged to $R_{wP} \approx 18\%$. The refinement of the preferred orientation along the [010] and [012] directions dropped the R_{wP} factor to 10%. This compound is layered (along the *b* axis), and it crystallizes as fine needles. The high compaction level in the capillary induced preferred orientation with the needles mainly oriented along the rotation axis. The GSAS program allowed the use of the March−Dollase[35] correction, and the coefficients converged to 2.181(15) (fraction = 0.5) for [010] and 0.841(4) (fraction = 0.5) for [012]. The refined peak shape parameters were: $LX = 0.23(3)$, $LY = 8.86(32)$, $S/L = 0.0099(3)$, $H/L = 0.0080(3)$, stec = 12(1), and ptec = 15.9(7). These parameters indicate that the peak shape is anisotropic with a significant broading along the [010] direction. Finally, an isotropic temperature factor was refined for each atom. The last refinement converged to $R_{wP} = 9.76\%$, $R_P = 7.82\%$ and $R_F = 6.83\%$; R factors are as defined by Rietveld[36] and by Larson and Von Dreele,[31] with a final weighting factor for the soft constraints of −40.

Table 1. Crystallographic Data for α-$Al(HO_3PC_6H_5)(O_3PC_6H_5){\cdot}H_2O$

fw	359.17	D_c/g cm^{-3}	1.702
cryst system	orthorhombic	λ/Å	0.39989(2)
a/Å	9.7952(1)	no. of overall params	104
b/Å	29.3878(4)	R_{wP}	0.098
c/Å	9.3537(3)	R_P	0.078
V/Å^3	2692.5(1)	R_F	0.068
Z	8	χ^2	1.65
space group	*Pbca* (No.61)		

Table 2. Positional Parameters and U_{iso} Values for α-$Al(HO_3PC_6H_5)(O_3PC_6H_5){\cdot}H_2O$

atom	*x*	*y*	*z*	U_{iso}/Å^2
Al	0.73354(30)	0.25023(14)	0.4060(7)	0.003(1)
P(1)	0.68796(28)	0.32379(9)	0.1780(5)	0.011(1)
P(2)	0.43969(31)	0.21105(9)	0.3315(5)	0.006(1)
O(1)	0.5356(4)	0.33016(17)	0.2214(9)	0.015(3)
O(2)	0.7021(6)	0.29836(19)	0.0367(6)	0.015(3)
O(3)	0.7663(6)	0.30042(19)	0.3006(7)	0.012(3)
O(4)	0.0796(4)	0.23214(16)	0.2093(10)	0.003(2)
O(5)	0.3375(5)	0.2158(20)	0.2073(7)	0.013(3)
O(6)	0.3842(7)	0.23097(18)	0.4710(6)	0.012(3)
O(7)	0.6111(7)	0.28812(21)	0.5263(14)	0.013(2)
C(1)	0.7595(7)	0.38058(11)	0.1566(8)	0.016(4)
C(2)	0.8507(9)	0.38883(18)	0.0455(10)	0.012(4)
C(3)	0.9028(11)	0.43268(23)	0.0270(13)	0.016(4)
C(4)	0.8419(11)	0.46916(16)	0.0980(13)	0.030(5)
C(5)	0.7465(10)	0.46090(15)	0.2047(13)	0.017(4)
C(6)	0.6977(9)	0.41682(16)	0.2269(12)	0.027(4)
C(7)	−0.0320(6)	0.15042(11)	0.1391(9)	0.008(4)
C(8)	0.5782(8)	0.12977(17)	0.2935(14)	0.017(4)
C(9)	0.5978(9)	0.08299(18)	0.3073(15)	0.013(4)
C(10)	0.5002(10)	0.05664(13)	0.3774(15)	0.022(4)
C(11)	0.3928(11)	0.07789(20)	0.4488(15)	0.035(5)
C(12)	0.3667(7)	0.12412(17)	0.4227(13)	0.005(4)

Crystallographic data for the refinement of α-$Al(HO_3PC_6H_5)(O_3PC_6H_5){\cdot}H_2O$ are given in Table 1. Final atomic and isotropic thermal parameters for **III** are given in Table 2, and bond lengths and angles, in Table 3. The final observed, calculated, and difference profiles are given in Figure 9. The coordination around the Al and P atoms is given in Figure 10, where all atoms are labeled. The arrangement of atoms in a layer and the packing of layers down the *a* axis are shown in Figures 11 and 12, respectively. The aluminum atoms have an octahedral environment of oxygens, five belonging to five different phosphonate groups and the sixth being the oxygen of the water molecule, O(7). There are two crystallographically independent phosphonate groups, one being protonated, P(1). The O(1) oxygen atom is the hydrogen phosphonate oxygen

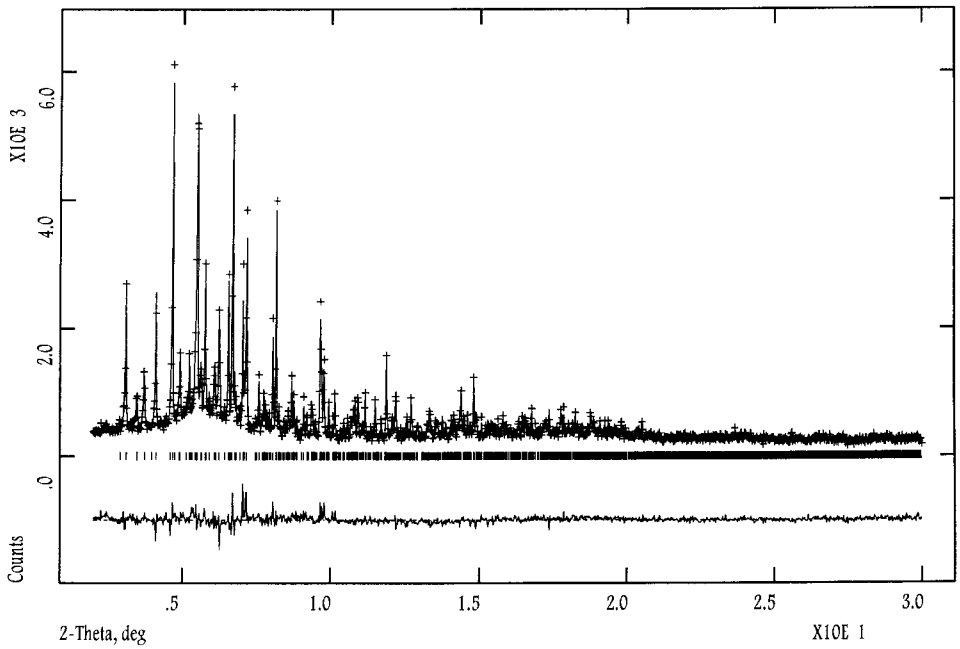

Figure 9. Observed, calculated, and difference synchrotron X-ray ($\lambda \approx 0.4$ Å) powder diffraction profiles for α-Al($HO_3PC_6H_5$)($O_3PC_6H_5$)·H_2O between 2 and 30° (2θ). The tic marks are calculated 2θ angles for Bragg peaks.

Table 3. Bond Lengths (Å) and Angles (deg) for α-Al($HO_3PC_6H_5$)($O_3PC_6H_5$)·H_2O

Al−O(2)	1.905(7)	O(2)−Al−O(3)	173.2(5)	O(3)−Al−O(7)	87.6(4)
Al−O(3)	1.803(7)	O(2)−Al−O(4)	91.48(28)	O(4)−Al−O(5)	87.5(4)
Al−O(4)	1.929(9)	O(2)−Al−O(5)	92.69(29)	O(4)−Al−O(6)	177.7(5)
Al−O(5)	1.786(6)	O(2)−Al−O(6)	87.5(4)	O(4)−Al−O(7)	89.96(31)
Al−O(6)	1.951(6)	O(2)−Al−O(7)	87.6(4)	O(5)−Al−O(6)	94.57(26)
Al−O(7)	1.986(10)	O(3)−Al−O(4)	93.4(4)	O(5)−Al−O(7)	177.5(5)
		O(3)−Al−O(5)	92.2(4)	O(6)−Al−O(7)	87.5(4)
		O(3)−Al−O(6)	87.49(28)		
P(1)−O(1)	1.558(3)	O(1)−P(1)−O(2)	111.81(29)	O(1)−P(1)−C(1)	106.70(23)
P(1)−O(2)	1.525(4)	O(1)−P(1)−O(3)	109.70(30)	O(2)−P(1)−C(1)	108.59(26)
P(1)−O(3)	1.541(4)	O(2)−P(1)−O(3)	112.40(26)	O(3)−P(1)−C(1)	107.37(27)
P(1)−C(1)	1.821(3)				
P(2)−O(4)	1.552(4)	O(4)−P(2)−O(5)	110.7(4)	O(4)−P(2)−C(7)	107.02(22)
P(2)−O(5)	1.540(4)	O(4)−P(2)−O(6)	111.77(30)	O(5)−P(2)−C(7)	107.38(26)
P(2)−O(6)	1.529(4)	O(5)−P(2)−O(6)	112.25(25)	O(6)−P(2)−C(7)	107.43(27)
P(2)−C(7)	1.824(3)				
P(1)−O(2)−Al	159.8(6)	P(1)−O(3)−Al	133.1(4)	P(2)−O(4)−Al	131.5(6)
P(2)−O(5)−Al	150.3(4)	P(2)−O(6)−Al	151.6(5)		

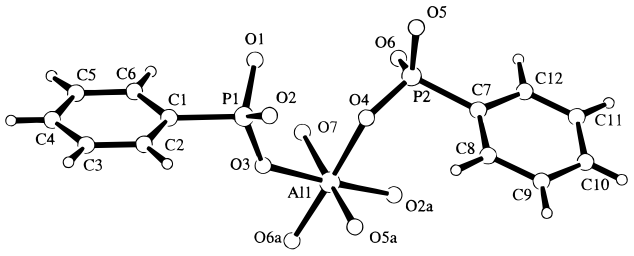

Figure 10. The atoms in one asymmetric unit of α-Al($HO_3PC_6H_5$)($O_3PC_6H_5$)·H_2O showing the octahedral environment around the Al.

and does not bond to the metal atoms. As observed in metal hydrogen phosphates[2] and hydrogen phosphonate compounds, the P(1)−O(1)H bond is longer than the other P−OM bonds (Table 3). Both phosphonate groups show the regular tetrahedral geometry typical of such groups, O_3PC. Inside an inorganic layer, two oxygen atoms, O(2) and O(3) that belong to P(1), link two consecutive aluminum atoms in the *c*-axis direction, giving rise to infinite Al···P(1)···Al chains. The phosphonate P(1) groups alternatively point the phenyl and the hydroxyl groups up and down the chains. These chains are also bridged by the P(2) atoms and then interconnected through the O(4) oxygen to give rise to the inorganic layer. This phosphonate group has the phenyl ring approximately perpendicular to the layers. The stacking of layers along the *b* axis is evident in Figure 12.

(c) Al($HO_3PC_6H_5$)$_3$·H_2O. The X-ray powder diffraction pattern of **V** was indexed, using the program TREOR90, in a monoclinic unit cell with the parameters $a = 8.402(3)$ Å, $b = 29.082(9)$ Å, $c = 9.176(4)$ Å, $\beta = 110.19(3)°$, $V = 2104.3$ Å^3, $Z = 4$, and $V_{at} = 16.4$ Å^3/atom (Table 4). The X-ray powder pattern was recorded with a sample diluted and blended with spherical particles of Cab-O-Sil M-5 (from Fluka), to reduce the preferred orientation.[37]

(d) Al(OH)($O_3PC_6H_5$). The X-ray powder diffraction pattern of **VI** was indexed in a monoclinic unit cell with the parameters $a = 16.400(3)$ Å, $b = 5.530(1)$ Å, $c = 8.270(3)$ Å, $\beta = 90.51(2)°$, $V = 750$ Å^3, $Z = 4$, and $V_{at} = 15.6$ Å^3/atom (Table 5). Both the TREOR90 and Lattparm programs converged to the same solution. The X-ray powder pattern was recorded as described above to reduce the preferred orientation.

^{27}Al and ^{31}P MAS NMR Study. ^{27}Al MAS NMR and ^{31}P

Table 4. X-ray Powder Diffraction Data for $Al(HO_3PC_6H_5)_3 \cdot H_2O$[a]

d_{obs}/Å	d_{cal}/Å	*hkl*	$I/I_m \times 100$
14.542	14.526	020	100.0
7.617	7.603	110	11.89
7.279	7.263	040	1.51
6.969	6.967	$\bar{1}11$	0.93
6.109	6.111	130	1.91
5.766	5.766	$\bar{1}31$	1.12
5.560	5.555	041	2.85
4.945	4.945	111	7.89
4.843	4.842	060	5.65
4.685	4.676	150	2.04
4.435	4.436	$\bar{1}12$	9.98
4.225	4.222	061	2.28
4.070	4.073	132	3.44
4.014	4.014	$\bar{1}61$, $\bar{2}21$	8.99
3.941	3.938	200, 032	2.27
3.803	3.801	220	2.53
3.669	3.672	170	2.67
3.620	3.632	$\bar{2}41$, $\bar{2}21$	6.43
3.484	3.488	161	4.43
3.348	3.347	081	3.40
3.305	3.3076	112	2.40

[a] $a = 8.402(3)$ Å, $b = 29.082(9)$ Å, $c = 9.176(4)$ Å, $\beta = 110.19(3)°$, $V = 2104$ Å^3, $V_{at} = 16.4$ Å^3/atom $Z = 4$.

Table 5. X-ray Powder Diffraction Data for $Al(OH)(O_3PC_6H_5)$[a]

d_{obs}/Å	d_{cal}/Å	*hkl*	$I/I_m \times 100$
16.443	16.434	100	100.0
5.481	5.474	300	0.52
4.600	4.597	011	3.16
4.426	4.423	111	8.46
4.104	4.102	400	10.13
4.015	4.016	$\bar{2}11$, $\bar{1}02$	9.04
3.708	3.707	$\bar{2}02$	2.27
3.512	3.509	311	6.02
3.313	3.317	$\bar{3}02$	2.15
3.283	3.285	302	2.79
3.055	3.0670	$\bar{4}11$	1.66
2.927	2.926	$\bar{4}02$	0.81
2.900	2.899	402	0.47
2.766	2.764	020	0.95
2.730	2.726	120	1.86
2.621	2.620	220	0.83
2.558	2.558	502	0.51
2.444	2.442	$\bar{1}13$	1.07
2.345	2.342	700, 611	1.26
2.291	2.289	$\bar{6}02$	0.53
2.278	2.277	$\bar{1}22$	0.55

[a] $a = 16.400(3)$ Å, $b = 5.530(1)$ Å, $c = 8.270(3)$ Å, $\beta = 90.51(2)°$, $V = 750$ Å^3, $V_{at} = 15.6$ Å^3/atom, $Z = 4$.

MAS NMR spectra for **I** are shown in Figure 13 (a) and Figure 14 a, respectively. The ^{27}Al spectrum for **I** shows two main broad peaks at 44 and −21 ppm with differently shaped shoulders, which correspond to aluminums in tetrahedral and octahedral coordinations, respectively (Figure 13a). The ^{31}P spectrum for **I** is formed by three components at −3, −6, and −8 ppm, due to at least three inequivalent O_3PC tetrahedral groups (Figure 14a).

^{27}Al MAS NMR spectra for **III** and **V** are shown in Figure 13b and Figure 13c, respectively. The ^{27}Al spectrum for **III** shows a sharp peak at −13.1 ppm, typical of aluminum with an octahedral oxygen environment. The ^{27}Al spectrum for **V** shows a broad asymmetric band at −20 ppm, due again to octahedral aluminum. In this case, three maxima are detected at −16.4, −19.9, and −23.9 ppm, which are produced by second-order quadrupolar interactions of a single aluminum with the electric field gradient at the nuclear metal site.

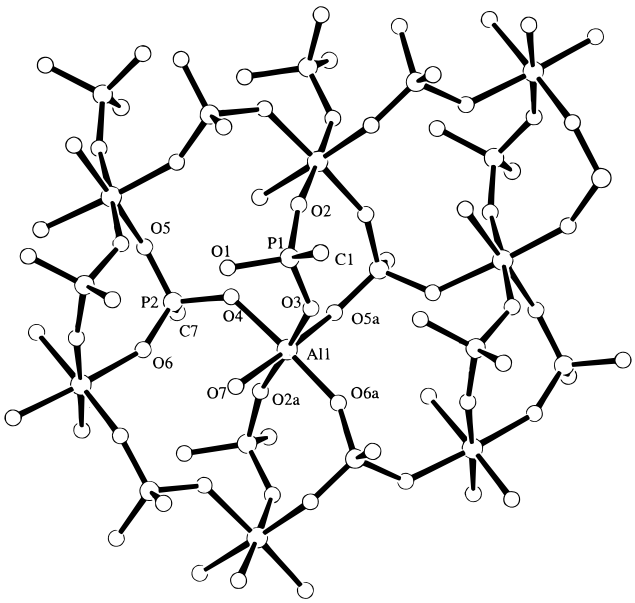

Figure 11. View of a layer of α-$Al(HO_3PC_6H_5)(O_3PC_6H_5) \cdot H_2O$ (*ac* plane) with atoms labeled.

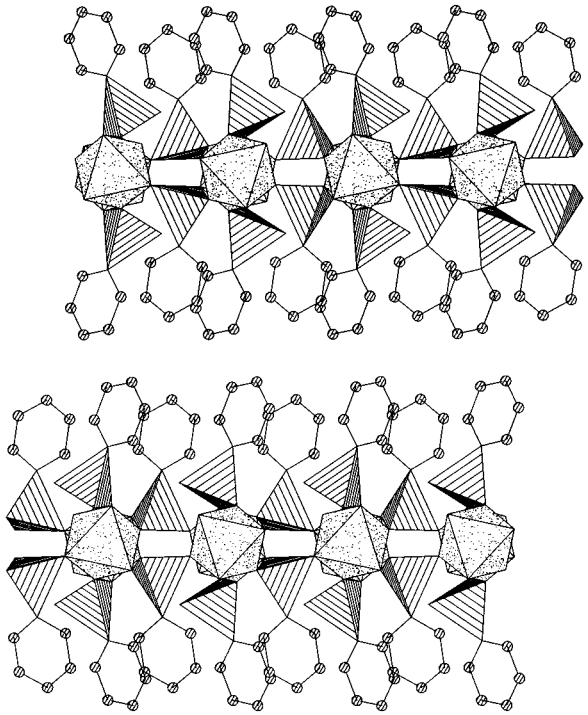

Figure 12. Three-dimensional packing of layers for α-$Al(HO_3PC_6H_5)(O_3PC_6H_5) \cdot H_2O$ down the *a* axis (*b* axis vertical).

^{31}P MAS NMR spectra for **III** and **V** are displayed in Figure 14b and Figure 14c, respectively. The ^{31}P spectrum for **III** shows a broad band at 1 ppm, which is the result of two partially overlapped signals at 1.5 and 0.3 ppm. The ^{31}P spectrum for compound **V** shows two broad bands at 5.1 and 1.7 ppm. The first band has double the intensity of the second one. A third small peak is observed at 19 ppm, which is probably due to an impurity.

Discussion

The crystal structures of several metal phenylphosphonates are known from single-crystal or powder diffraction studies. Layered materials, independently of the metal cation size, the

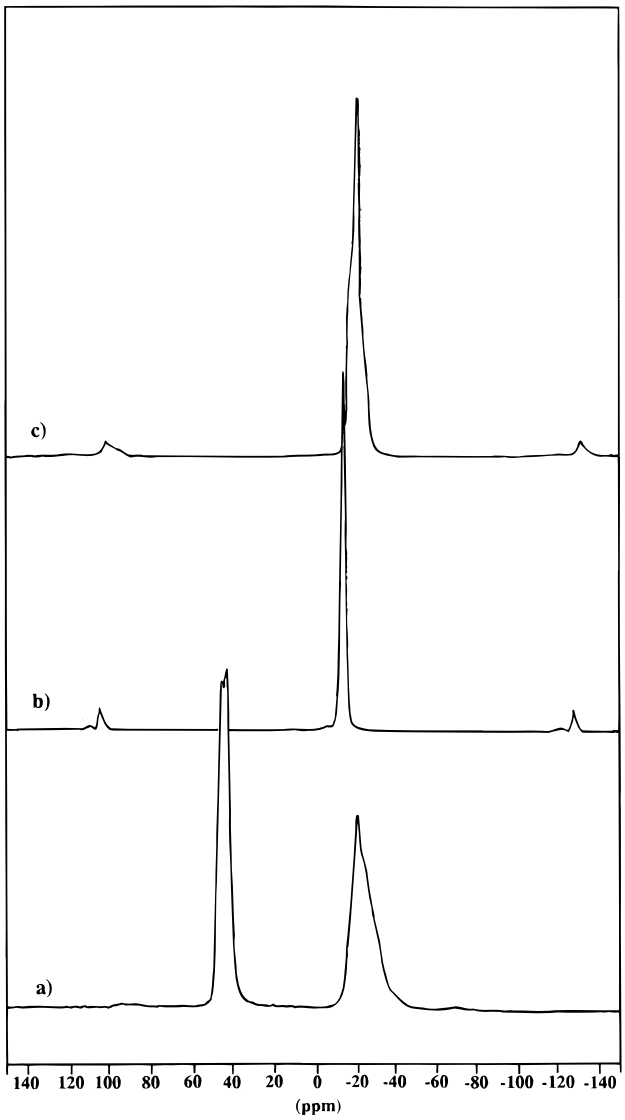

Figure 13. ^{27}Al MAS NMR spectra for (a) $Al_2(O_3PC_6H_5)_3 \cdot 2H_2O$, (b) α-$Al(HO_3PC_6H_5)(O_3PC_6H_5) \cdot H_2O$, and (c) $Al(HO_3PC_6H_5)_3 \cdot H_2O$.

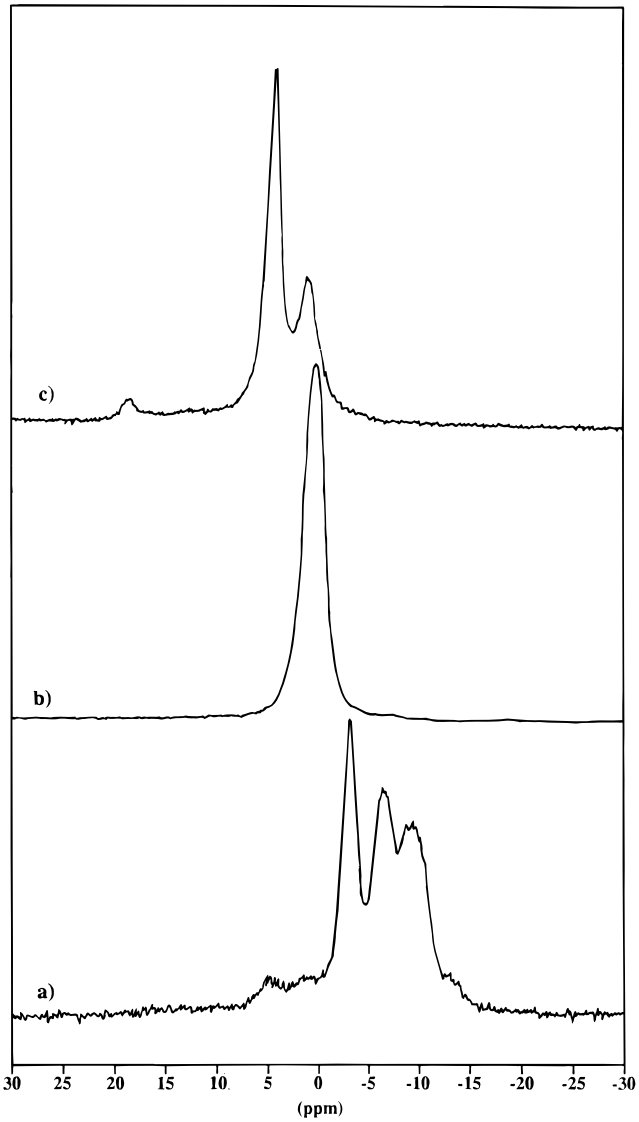

Figure 14. ^{31}P MAS NMR spectra for (a) $Al_2(O_3PC_6H_5)_3 \cdot 2H_2O$, (b) α-$Al(HO_3PC_6H_5)(O_3PC_6H_5) \cdot H_2O$, and (c) $Al(HO_3PC_6H_5)_3 \cdot H_2O$.

metal coordination polyhedra, and the metal/phosphonate molar ratio, always display a strong diffraction peak at ∼15 Å characteristic of an organic bilayer of phenyl groups between an inorganic layer formed by the metal−phosphonate bonding. For example peaks at 15.7 Å for $La^{III}(HO_3PC_6H_5)(O_3PC_6H_5)$,[10] 15.6 Å for $Pb^{II}(HO_3PC_6H_5)_2$,[38] 14.8 Å for $Zr^{IV}(O_3PC_6H_5)_2$,[3] and 14.33 Å for $Mn^{II}(O_3PC_6H_5) \cdot H_2O$[5] are known for layered metal phenylphosphonates. Although the crystal structures of three polymorphs of $Fe^{III}(HO_3PC_6H_5)(O_3PC_6H_5) \cdot H_2O$ are not known, the main *d* spacings range from 14.66 to 15.11 Å, indicating that these are also probably layered materials.[9] The most intense peaks of $Al^{III}(HO_3PC_6H_5)(O_3PC_6H_5) \cdot H_2O$ and $Al_2{}^{III}(O_3PC_6H_5)_3 \cdot 4H_2O$ were reported at 14.8 Å[25] and 14.35 Å,[26] respectively, and the authors suggested layered structures.

The structure of **III** has been solved ab initio from powder diffraction data; it is layered with the main peak at 14.7 Å, representing the basal spacing. Compound **IV**, with the main peak at 14.8 Å, is a polymorph of the α-phase with a very related layered structure. The existence of several polymorphs depending on the synthetic conditions is quite common in the chemistry of metal phosphonates. Even the nature of the salt that is the source of the metal cation may slightly affect the structure of the final product.[24]

On the other hand, several attempts to solve the structures of **V** and **VI** from laboratory X-ray powder diffraction data have been unsuccessful. However, the patterns present strong preferred orientation effects and main peaks at 14.6 and 16.4 Å, respectively, which suggests layered structures.

The ^{27}Al MAS NMR spectrum for **III** shows a single peak due to a distorted octahedral environment of oxygens at −13.1 ppm, in agreement with the single-crystal structural analysis. Quadrupolar constants deduced from the experimental profile of this peak were $C_Q = 0.23$ MHz and $\eta = 0$. The ^{31}P MAS NMR spectrum for **III** shows a broad peak due to two signals at 1.5 and 0.3 ppm, which correspond to the nonresolved HO_3P-(1)C and O_3P(2)C groups, respectively. In a first approximation, the hydrogen phosphonate groups are expected to be at higher chemical shifts than the corresponding phosphonate groups. Typical variations of 3−6 ppm are observed between monohydrogen phenylphosphonate and phenylphosphonate groups.[39] However, some other factors can affect the ^{31}P signal position such as the P−C and P−O bond distances, the POAl angles, and even the van der Waals interactions between phenyl rings.

(37) Aranda, M. A. G.; Cabeza, A.; Bruque, S.; Poojary, D. M.; Clearfield, A. *Inorg. Chem.* **1998**, *37*, 1827−1832.

The result of these factors appears to prevent the resolution of the two overlapped ^{31}P signals.

The ^{27}Al MAS NMR spectrum for **V** has a band composed of three maxima that correspond to the same distorted octahedron. From the analysis of the experimental profile, the values of the quadrupolar constants were $C_Q = 0.37$ MHz and $\eta = 1$. The ^{31}P MAS NMR spectrum for **V** shows two broad bands at 5.1 and 1.7 ppm, which must be due to at least three signals, as the peak at 5.1 ppm has double the intensity of that at 1.7 ppm. The peak at lower chemical shift must correspond to one crystallographically independent phosphorus atom in a general position. Then, the peak at 5.1 ppm must be the result of two overlapped signals of the same intensity. These spectra are again compatible with a layered framework of strongly distorted octahedral aluminums sanwiched between hydrogen phenylphosphonate tetrahedral groups.

Compound **I** has the main diffraction peak at 13.2 Å, being the second-order reflection of the first peak observed at 26.4 Å. In contrast to what happens for compounds **III** and **V**, where the main peak does not change on heating, the main peak of **I** decreases from 13.2 to 11.7 Å suggesting a different structure from that proposed for $Al_2(O_3PC_6H_5)_3 \cdot 4H_2O$.[26] The relationship between the powder patterns of **I** and **II** (Figure 2) indicates a topotactic dehydration that we have found to be reversible. This dehydration process takes place at a very low temperature ~60 °C which indicates a labile water that is weakly retained. The powder patterns have broad peaks probably due to a small microcrystal average size. However, some insights about the structure may be derived by comparing the X-ray and MAS NMR results with those published for related materials.

The ^{27}Al MAS NMR spectrum for **I** has two bands due to octahedral (−21 ppm) and tetrahedral (46 ppm) oxygen environments. A similar spectrum is observed for β-$Al_2(O_3PCH_3)_3 \cdot H_2O$[23] with two signals, at −17.6 and 41.2 ppm. This compound crystallizes in a trigonal cell of dimensions $a = 24.65$ Å, $c = 25.30$ Å, $\gamma = 120$ °, and $Z = 36$. The structure is tubular with small channels running parallel to the c axis and the methyl groups projected toward the interior of the channels resulting in a microporous material with tunnels of approximately 5.8 Å of cross-section. The relationship between the unit cells and mainly the very similar ^{27}Al MAS NMR spectra suggest that **I** has a related tubular structure. However, N_2 adsorption−desorption isotherms showed that no micropores are present in this material. The analysis of these data yielded a low specific BET surface area (25 m^2/g). The existence of different maxima detected in the corresponding ^{31}P and ^{27}Al signals suggests that the numbers of crystallographic sites are higher than the chemical formula (three P and two Al). From the analysis of the ^{27}Al envelope, the presence of two tetrahedral and two octahedral environments for Al was deduced. For the ^{31}P signal, the three detected components exhibit different line widths, probably indicating the existence of more than three components. A determination of quadrupolar constants is difficult due to the overlapping of signals. These results are compatible with the powder diffraction study, as the very large unit cell ($V = 19440$ Å^3) may contain several nonequivalent P and Al sites. However, the indexation of the powder pattern of this material is only a preliminary result, and further study with a better crystallized sample is necessary.

The ^{31}P MAS NMR study of three aluminum phenylphosphonates with different stoichiometries has revealed a clear trend. **I** has no hydrogen phosphonate groups and the ^{31}P signals range between −2 and −9 ppm. **III** has a hydrogen phosphonate and a phosphonate group with a broad peak centered at 1 ppm. **V** has three hydrogen phosphonate groups with peaks ranging between 5 and 2 ppm. The influence of the HO−P groups in the positions of the ^{31}P signals is, hence, clearly observed. As should be expected, a shift in the ^{31}P signal position to higher positive chemical shift values occurs as the phosphonate groups become more protonated.

It is important to underline the thermal stabilities of these types of phosphonates. **I** dehydrates quickly above 60 °C but **II** remains stable up to 550 °C. Above this temperature, it undergoes combustion in air. **III** and **V** lose crystallinity after the dehydration processes at 180 and 240 °C, respectively. The water is bonded to the aluminum atom in **III**, and the high temperature at which water is lost in **V** supports that water is bonded to Al, in the same way that is observed in **III**. Both compounds undergo pyrolysis above 400 °C in the atmosphere. The temperature of the water loss processes and the ν_{O-H} stretching vibration frequencies indicate that water is weakly retained in **I**, it is strongly bonded in **III**, and it presents the strongest interaction in **V**. Finally, compound **VI** undergoes condensation of the hydroxide groups at 280 °C. Then it remains stable up to 600 °C, whereas the combustion of the organic matter in air takes place.

In the course of this investigation, other slightly different aluminum phenylphosphonates have been obtained. A full characterization of these compounds is in progress and will be reported elsewhere. It is noteworthy that minor changes in the syntheses lead to different stoichiometries and/or structures.

Acknowledgment. We thank NATO for funding through NATO CRG Program 951242. The work in Málaga was also supported by Research Grants FQM-113 of Junta de Andalucía (Spain) and MAT-97-326-C4-4 of CICYT, Ministerio de Educación y Ciencia, Spain. We also thank Drs. E. Dooryhee, G. Vaugahn, and A. Fitch for assistance during data collection on BM16 and the ESRF for the provision of synchrotron facilities. A.C. wishes to thank the Robert A. Welch Foundation for partial support of this effort under Grant No. A-673.

IC9802350